

On the lattice Boltzmann method for phonon transport

Aydin Nabovati*, Daniel P. Sellan, Cristina H. Amon

Department of Mechanical & Industrial Engineering, University of Toronto, Toronto, Ontario, Canada M5S 3G8

ARTICLE INFO

Article history:

Received 5 July 2010

Received in revised form 31 January 2011

Accepted 31 March 2011

Available online 16 April 2011

Keywords:

Lattice Boltzmann method

Phonon transport

Heat transfer

ABSTRACT

The lattice Boltzmann method is a discrete representation of the Boltzmann transport equation that has been employed for modeling transport of particles of different nature. In the present work, we describe the lattice Boltzmann methodology and implementation techniques for the phonon transport modeling in crystalline materials. We show that some phonon physical properties, e.g., mean free path and group velocity, should be corrected to their effective values for one- and two-dimensional simulations, if one uses the isotropic approximation. We find that use of the $D2Q9$ lattice for phonon transport leads to erroneous results in transient ballistic simulations, and the $D2Q7$ lattice should be employed for two-dimensional simulations. Furthermore, we show that at the ballistic regime, the effect of direction discretization becomes apparent in two dimensions, regardless of the lattice used. Numerical methodology, lattice structure, and implementation of initial and different boundary conditions for the $D2Q7$ lattice are discussed in detail.

© 2011 Elsevier Inc. All rights reserved.

1. Introduction

The conventional continuum-based physical relations that describe heat and fluid flow in bulk systems, such as the Navier–Stokes and Fourier equations, break down at sub-continuum scales [1,2]. The failure of these relations, along with the current trend of miniaturization in man-made devices and wide spread use of nano-structured systems, urge for development of new computational techniques capable of modeling sub-continuum physical phenomena. One example of such techniques is the phonon lattice Boltzmann method that has been developed to model thermal transport in devices with sub-continuum feature sizes.

In current semiconductor technology, the feature size of transistors on an integrated circuit is about 32 nm, and the projected size in the next generation of devices is advancing below that. This continued miniaturization of electronic components subsequently results in higher heat generation densities inside the device. Non-uniform power distribution across the die surface, and sub-continuum effects cause large temperature gradients and localized hot spots on the die. This overheating of the die surface hinders the performance and reliability of these devices; and therefore, makes thermal management a crucial step for further developments [3].

In semiconductor materials, atomic lattice vibrations are the dominant heat carriers; the quantum of these atomic vibrations is a phonon [4]. In devices with feature sizes comparable to the bulk mean free paths of phonons (on average a few tens to hundreds of nanometers), phonons travel ballistically. In this ballistic regime, phonon-boundary scattering overshadows intrinsic phonon scattering and dominates thermal transport. As a result, sub-continuum boundary effects appear as (i) temperature jumps at the system boundaries, and (ii) a size-dependent thermal conductivity. The conventional Fourier-based methods for modeling bulk thermal transport fail to capture these ballistic effects; therefore, the study of phonon behavior

* Corresponding author. Tel.: +1 416 946 8216; fax: +1 416 978 7753.

E-mail address: a.nabovati@utoronto.ca (A. Nabovati).

becomes crucial for accurate predictions of thermal transport at such scales [5,6]. Different numerical methods have been proposed in the literature for phonon transport modeling through solving the Boltzmann transport equation (BTE).

Joshi and Majumdar developed an equation for phonon radiative transfer that was based on the BTE and employed average phonon properties [7]. Chen proposed a Ballistic-Diffusive equation for phonon transport; where the phonon distribution function was divided into two components, ballistic and diffusive [8,9]. Narumanchi et al. employed the finite volume method to solve the BTE for thermal transport modeling in electronic devices using mode-dependent phonon properties [10,11]. Monte Carlo simulations have also been applied to solve the BTE and obtain phonon distribution in nano-scale devices [12–14].

Another approach for solving the BTE, which is adopted in the present work, is the lattice Boltzmann method (LBM). The LBM is a particle-based method, which uses a finite differencing technique to numerically solve the BTE, and predicts the distribution of particles in discrete directions on discrete points in time and space [15]. Chronologically, the LBM was first introduced in the work of McNamara and Zanetti [16] as a fluid flow modeling technique through prediction of the distribution of fictitious fluid particles, which was then extended in the works of other researchers [17–19]. Benzi et al. [20] and Chen and Doolen [21] have provided comprehensive reviews on the LBM for fluid flow simulation. Since then, the LBM has also been employed for modeling transport of electrons and phonons, the latter is studied in the present work. Guyer [22] introduced a lattice Boltzmann computational framework for modeling transport of different phonon modes using a two-dimensional hexagonal lattice, i.e., $D2Q7$ lattice (the lattice labeling is discussed in Section 3.1). Jiaung and Ho developed a lattice Boltzmann computational framework for modeling phonon hydrodynamics [23,24]. In the phonon hydrodynamics approach, similar to the classical fluid quasi-particles in the LBM for fluid flow, phonons are assumed to be constituent particles of a quantum fluid. Recently, Yang and Hung [25] also developed a lattice Uehling–Uhlenbeck Boltzmann method for modeling the behavior of quantum fluids. In their proposed approach, the quantum particles were assumed to follow the Uehling–Uhlenbeck Boltzmann equation [26,27] and they examined the behavior of particles under three different equilibrium distribution functions. The phonon hydrodynamics approach developed in the works of Jiaung and Ho [23,24] and Yang and Hung [25] cannot be extended to include multiple phonon modes. Furthermore, the phonon properties in these works are chosen arbitrarily and do not correspond to any physically meaningful material property.

Atomistic level modeling techniques have shown that phonon properties are closely related to atomic structure of materials and cannot be chosen arbitrarily [28–32]. Therefore, instead of using the phonon hydrodynamics approach, we treat phonons as quasi-particles, where their properties are directly related to material structure. Most of the recent works on the LBM for phonon and electron transport modeling have adopted this approach, which can also be extended to include multiple phonon modes.

This approach for LBM was first introduced by Ghai et al. [33], where they used the LBM for coupled modeling of phonons and electrons in semiconductor materials and metals. Their LBM for phonons was further developed in the works of Escobar et al. [34–36] and Goicochea et al. [37–39]. These latter works employed the $D2Q9$ lattice with multiple phonon modes. Thouy et al. [40,41] performed single- and multi-mode phonon LBM simulations on a $D2Q9$ lattice; in order to have a higher resolution for direction sampling, they further developed their model to include 24 different direction, i.e., $D2Q25$ lattice. Heino has also performed nano-scale heat transfer simulations using the mode-dependent LBM on a $D2Q9$ lattice [42–44]. Recently, Christensen and Graham [45] developed a coupled LBM/finite difference method to model the heat transfer in joint micro- and macro- domains.

In spite of multiple works that have been published on the phonon LBM, the current literature lacks a comprehensive piece of work that solely explains the methodology and its numerical implementation. Furthermore, the effect of lattice structure on the predicted results, and the use of effective phonon properties in one- and two-dimensional simulations have not been addressed in the literature.

The present work explains the LBM for phonon transport in one- and two-dimensions. The detailed methodology is discussed in Section 2. Section 3 presents the numerical implementation of the LBM; where effective phonon properties for one- and two-dimensional simulations, and effect of different lattice structures on the predicted results are discussed in Sections 3.2 and 3.3, respectively. Numerical examples are presented to demonstrate the methodology and implementation in Section 4. For interested readers, streaming rules, and implementation of initial and boundary conditions for a $D2Q7$ lattice are discussed in detail in the Appendices.

2. Lattice Boltzmann methodology

The BTE with single relaxation time assumption (Bhatnagar–Gross–Krook assumption [46]) and in absence of any external force is given as follows:

$$\frac{\partial f}{\partial t} + \mathbf{v}_g \cdot \nabla f = \frac{f^{eq} - f}{\tau} \quad (1)$$

where t is time; f , \mathbf{v}_g , and τ are the probability distribution function, group velocity vector, and relaxation time of the particles under study [15]. f^{eq} is the equilibrium particle distribution function, and depends on the nature of the particles which are to be described by the BTE. The corresponding equilibrium distribution functions for classical particles (e.g., fluid particles), fermions (e.g., electrons), and bosons (e.g., photons and phonons) are given by the Maxwell–Boltzmann, Fermi–Dirac,

and Bose–Einstein distribution functions, respectively [47]. Among them, the Bose–Einstein equilibrium distribution function for phonons is given as follows:

$$f^{eq} = \frac{1}{e^{h\omega/k_b T} - 1} \quad (2)$$

where h is the Planck's constant divided by 2π , ω is the frequency of phonons (*rad/s*), k_b is the Boltzmann constant, and T is the absolute temperature.

Most of the previous works on the phonon LBM have assumed isotropic material properties, i.e., the atomic crystal is uniform in all directions. In isotropic materials, the group velocity vector of each phonon mode, \mathbf{v}_g , reduces to a scalar value, v_g , which is the speed of sound in the material of interest. Sellan et al. compared the results of the multi-mode isotropic assumption to those obtained considering all of the phonons in the first Brillouin-zone with anisotropic properties in an LBM framework [48]; they found that the isotropic assumption introduces an error up to 25% in the predicted cross-plane thermal conductivity of Stillinger–Weber silicon thin films.

Based on the treatment of different phonon modes, the LBM for phonon transport is divided into two main categories, namely: multi-mode LBM (Dispersion LBM) and single-mode LBM (Gray LBM). The Dispersion LBM solves the BTE for each phonon mode, where each mode has a distinct group velocity and relaxation time. Given an interatomic potential that describes the atomic interactions, the mode-dependent group velocities can be predicted from harmonic lattice dynamics calculations [30,31]; while the required relaxation times can be predicted from empirical relations [49,50], molecular dynamics simulations [28,51], or anharmonic lattice dynamics calculations [52]. The Gray LBM for phonon transport, however, considers average phonon properties, and solves the BTE to predict the distribution function of only one representative phonon mode. It has been shown that in order to have an accurate prediction of the temperature distribution and heat flux, mode-dependent properties should be included in the calculations [35,36]. Recently, Turney et al. [52] and Sellan et al. [48,54] showed that using average phonon properties is inadequate for predicting the in-plane and cross-plane thermal conductivities of Stillinger–Weber silicon thin films.

The Dispersion LBM can be considered as solving a Gray LBM for multiple phonon modes, with minor modifications in numerical implementation. Since the objective of the present work is to discuss the methodology and implementation of the LBM for phonon transport, the Gray approximation has been adopted for the sake of simplicity and clarity. Extending the Gray LBM to the Dispersion LBM is straightforward, provided the group velocity and relaxation time of each phonon mode are known. Details regarding the implementation of the Dispersion LBM can be found elsewhere [37,53].

Assuming the Gray approximation, the first-order discretization of the BTE for phonons in time and space (under the relaxation time approximation) results in the discrete lattice Boltzmann equation [15]:

$$f_\alpha(\mathbf{x} + \Delta\mathbf{x}_\alpha, t + \Delta t) - f_\alpha(\mathbf{x}, t) = \frac{\Delta t}{\tau} [f_\alpha^{eq}(\mathbf{x}, t) - f_\alpha(\mathbf{x}, t)] \quad (3)$$

where \mathbf{x} is the position in space, and the subscript α represents the discretized directions on each lattice site. f_α and f_α^{eq} are the corresponding direction-wise phonon distribution function and equilibrium distribution function. Δt is the computational time step, which is related to the lattice spacing as $\Delta\mathbf{x}_\alpha = v_{g,\alpha}\Delta t$; where $v_{g,\alpha}$ is the group velocity along direction α (discrete velocity set).

At each time step during the LBM simulation, the distribution functions move in the direction of the assigned discrete velocity set towards the next lattice site (streaming step); and based on a set of collision rules, new distributions are calculated at each lattice site for the next time step (collision step). The effect of boundary conditions and external sources are also included in the computation of new components of distribution function on each lattice site at each time step during the collision step.

3. Numerical implementation

3.1. Overview

Since in the Gray approximation we consider only one representative mode with average phonon properties, all phonons have a uniform group velocity, v_g , and the same relaxation time, τ . Therefore, the computational domain discretization is uniform in space, and one single lattice with uniform spacing in all directions should be used for all the phonons. In the present work, we follow the lattice labeling conventions introduced by Qian et al. [18]; i.e., $DnQm$, where n is the dimensions of space and $m - 1$ is the number of directions on each lattice site. For one-dimensional simulations, the $D1Q3$ lattice geometry is straightforward to implement (Fig. 1(a)). Any lattice selection in two dimensions should be symmetric and plane-filling. Two possible lattice configurations, which have been extensively employed for the fluid flow simulation using the LBM, are the $D2Q7$ and $D2Q9$ lattice structures (Fig. 1(b) and (c), respectively).

For all lattice structures discussed in this work, the phonon population at the center (f_m) is reserved to keep the summation of all the phonon distribution functions on that lattice site,

$$f_m(\mathbf{x}, t) = \sum_{\alpha=1}^{m-1} f_\alpha(\mathbf{x}, t) \quad (4)$$

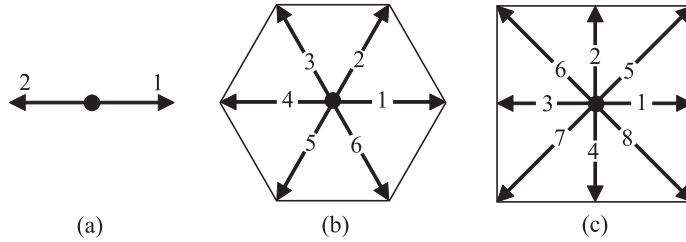


Fig. 1. (a) D1Q3, (b) D2Q7, and (c) D2Q9 lattice structures and respective labeling; the sites located at the center of the three lattices correspond to $\alpha = 3, 7,$ and $9,$ respectively.

3.2. Effective phonon properties

Considering the Gray approximation, phonons that leave a point in a three-dimensional space travel in all directions at a constant velocity magnitude of v_g , without any preference towards any specific direction. In two-dimensional simulations, phonons that are traveling in the three-dimensional space should be projected onto the two-dimensional plane of interest. Therefore, in calculating the average phonon velocity magnitude in the two-dimensional plane, the effect of the phonons which are out of the plane of interest should be taken into account. Fig. 2(a) schematically shows the three-dimensional phonon propagation and its projection into a two-dimensional plane, i.e., the x - y plane.

In a two-dimensional simulation in the x - y plane, consider an arbitrary direction with an angle ϕ with the x axis, i.e., the dark vector in Fig. 2(a). In order to calculate the average velocity of phonons in this direction, the effect of all the phonons that are traveling in this direction and are out of the x - y plane, which are shown as light vectors, should be considered. The plane of these phonons is marked in gray in Fig. 2(a), and is shown separately in Fig. 2(b).

This argument is true for any arbitrary direction in the two-dimensional x - y domain. Mathematically, it can be shown that the magnitude of the average projected phonon velocity ($v_{g,\phi}$) in an arbitrary direction in the x - y plane is $2/\pi$ of the physical velocity magnitude of a phonon in three dimensions;

$$v_{g,\phi} = \frac{1}{S} \int_S v_g \sin\theta ds = \frac{1}{\pi R} \int_0^\pi v_g \sin\theta R d\theta = \frac{2}{\pi} v_g \tag{5}$$

where R and S are the radius and length of the integration curve (semi-circle), and θ is the angle from z axis.

Therefore, for any two-dimensional simulation, the physical average group velocity and consequently the physical average mean free path of phonons ($\lambda = \tau v_g$) should be corrected by a factor of $2/\pi$. The same procedure should be applied when projecting the phonons from a three-dimensional domain into a one-dimensional domain. As a result of the integration, the phonon group velocity and mean free path to be used in one-dimensional simulations are those of three-dimensional space (physical values) corrected by a factor of $1/2$. All other physical phonon properties, including the relaxation time and specific heat, do not require a correction. These corrections factors are introduced in the phonon LBM literature for the first time.

3.3. Lattice structure: D2Q7 vs. D2Q9

Proper selection of the numerical lattice structure is also a concerning issue in two-dimensional LBM simulations. All the previous works on the phonon LBM modeling in two dimensions, except the work of Guyer [22], have preferred the D2Q9

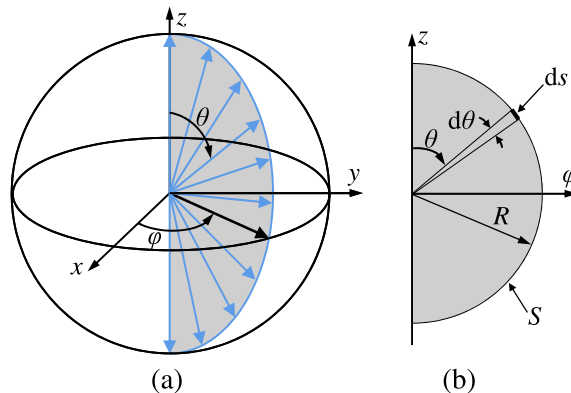


Fig. 2. Schematic projection of three-dimensional phonon propagation into a two-dimensional domain (x - y plane).

lattice over the $D2Q7$ structure for its simple structure and more straightforward boundary condition implementation [24,36,40,44,45].

The steady state temperature distribution in diffuse regime (i.e., bulk-like) obtained using the $D2Q9$ lattice has been shown to be in excellent agreement with analytical and numerical implementations of the Fourier heat equation [53]. However, no validation is reported in the literature for two-dimensional transient ballistic regime simulations using the LBM. The inherent problem with the $D2Q9$ lattice is that at each time step, the particles on diagonal directions (directions 5, 6, 7, and 8 in Fig. 1(c)) travel a distance $\sqrt{2}$ times larger than the distance travelled by the particles on the main directions (directions 1, 2, 3, and 4 in Fig. 1(c)). In the LBM for fluid flow simulations, this issue has been accounted for by altering the direction-wise velocities of the fictitious fluid particles and introducing a weight factor for particles moving in different directions. However, in the LBM for phonon transport with the Gray approximation, all the phonons have the same velocity in all directions. The same argument is true for isotropic multi-mode LBM, where phonons of each mode travel at a constant direction-independent velocity. Consequently, phonons in the diagonal direction cannot travel a larger distance than the phonons in the main directions at each time step. It is shown in the next section that this approximation in the $D2Q9$ lattice yields unrealistic results for transient simulations.

On a $D2Q7$ lattice, as it is shown in Fig. 1(b), the particles move on six equi-length directions separated from each other by an angle of $\pi/3$. Fig. 3 shows the $D2Q7$ lattice implementation on a two-dimensional domain. Considering the lattice orientation shown in Fig. 3, every other lattice site on the left and right boundaries does not fall on the physical domain boundaries. Boundary condition implementation on these two boundaries should be treated with extra care (see Appendices A and B). Geometrical constraints of the $D2Q7$ lattice implies that Δy is $\sqrt{3}\Delta x/2$. It also should be noted that a constant i line is a zigzag line, as shown in Fig. 3 (see Appendix C). The discrete velocity set for the $D2Q7$ lattice is given as follows:

$$v_{g,\alpha} = \left[\cos\left((\alpha - 1)\frac{\pi}{3}\right), \sin\left((\alpha - 1)\frac{\pi}{3}\right) \right] v_g \quad \alpha = 1, \dots, 6 \quad (6)$$

The streaming rules for the $D2Q7$ lattice implementation shown in Fig. 3 are presented in Appendix C.

3.4. Calculating thermal properties

On each lattice site, the distribution function has $m - 1$ direction-wise active components; and the equilibrium distribution function on that lattice site is calculated using the summation of all these $m - 1$ components. The equilibrium distribution function is assumed to be uniformly distributed on the $m - 1$ directions; therefore, on an arbitrary direction α , it is equal to:

$$f_{\alpha}^{eq}(\mathbf{x}, t) = \frac{\sum_{\beta=1}^{m-1} f_{\beta}(\mathbf{x}, t)}{m - 1} \quad \alpha = 1, 2, \dots, m - 1 \quad (7)$$

The reader should make distinction between the total equilibrium distribution on each node (calculated from the summation of all the $m - 1$ components of the distribution function, or from Eq. (2) if the temperature is known), f^{eq} , and its direction-wise components, f_{α}^{eq} ; these two are related as:

$$f^{eq}(\mathbf{x}, t) = \sum_{\alpha=1}^{m-1} f_{\alpha}^{eq}(\mathbf{x}, t) \quad (8)$$

Temperature on each lattice site is then calculated by solving Eq. (2) for T and using the calculated equilibrium distribution function on each lattice site, as follows:

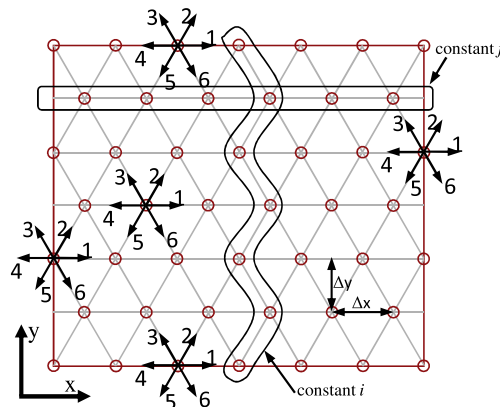


Fig. 3. $D2Q7$ lattice implementation and boundary lattice nodes.

$$T(\mathbf{x}, t) = \frac{\hbar\omega}{k_b \log\left(\frac{1}{f_{eq}(\mathbf{x}, t)} + 1\right)} \quad (9)$$

It should be noted that Eq. (9) is only valid for the Gray approximation; the methodology for the temperature calculation in the multi-mode LBM is described in Sellan et al. [48].

On each lattice site, heat flux in an arbitrary direction \mathbf{n} is calculated by writing the balance of energy for the ingoing and outgoing phonons. For an arbitrary direction \mathbf{n} , it is written as follows:

$$q_{\mathbf{n}}(\mathbf{x}, t) = \left[\sum (f_{in}(\mathbf{x}, t)\cos\theta - f_{out}(\mathbf{x}, t)\cos\theta) \right] \hbar\omega v_g D_{\omega} \Delta\omega d / \pi \quad (10)$$

where θ , D_{ω} , $\Delta\omega$, and d are the angle between the phonon's direction and the arbitrary direction \mathbf{n} , phonon's density of state, frequency bandwidth (equal to ω in Gray model), and dimension of space. The average phonon frequency, ω , is equal to $k_b T_D / \hbar$, where T_D is the Debye temperature and is equal to 625 K for silicon. The phonon density of states, D_{ω} , is calculated as follows:

$$D_{\omega} = \frac{c_v}{k_b \chi^2 e^{\chi} (e^{\chi} - 1)^{-2} \Delta\omega} \quad (11)$$

where c_v is the volumetric specific heat, and χ is $\hbar\omega/k_b T_{ave}$. Hereinafter, the coefficient $\hbar\omega v_g D_{\omega} \Delta\omega d / \pi$ in Eq. (10) is called q_{factor} for brevity. In all the above relations, the effective values of the mean free path and group velocity should be used.

The kinetic theory expression of bulk thermal conductivity of a Gray medium as a function of the average bulk phonon properties is given as follows [4]:

$$k_{bulk} = \frac{1}{3} c_v v_g A \quad (12)$$

The coefficient 1/3 is due to the averaging of the phonon velocities in space; therefore, only the physical values of the mean free path and group velocity should be used in Eq. (12) and no correction factor is required.

4. Numerical examples

4.1. Heat diffusion in a square domain with constant temperature boundary conditions

To validate our methodology, we modeled steady state diffuse-regime heat transfer in a square domain using both the *D2Q7* and *D2Q9* lattices and compared the predicted results against the analytical Fourier-based solution. The side length of the domain (L) was 5 μm and a lattice resolution study of the steady state results for the temperature profile (a scalar field) showed that at least 300 lattice sites on each side of the domain are required to have lattice-independent steady state simulations. It should be noted that, as a rule of thumb, the lattice resolution required to obtain lattice-independent steady state results for the heat flux (a vector field) or transient results for either temperature or heat flux is about 20 times higher than that required for capturing the correct steady state temperature profile. This lattice resolution corresponds to about 50 lattice sites per physical mean free path and is consistent with our previous findings for one-dimensional multi-mode LBM simulations. Therefore, we used a domain of 6001×6929 lattice sites for the *D2Q7* structure and a domain of 6001×6001 lattice sites for the *D2Q9* structure simulations. Furthermore, it was observed that the predicted values of heat flux requires a longer simulation time to reach the steady state when compared against the time required for obtaining the steady state temperature profile. This trend has also been reported in the molecular dynamics simulations [55].

The entire domain was initialized to a constant temperature of 299.5 K (T_c), whereas the temperature on the top boundary ($y/L = 1$) was set to a temperature of 300.5 K (T_h). Domain initialization and implementation of boundary conditions are explained in [Appendices A and B](#), respectively. The steady state temperature and heat flux in the y -direction profiles at three different y/L values of 0.25, 0.50, and 0.75, calculated using the LBM on the *D2Q7* and *D2Q9* lattices, are compared in [Fig. 4](#) against the values determined by the Fourier-based analytical solution [56]. It can be seen that for the steady state diffuse regime, both lattice structures perform well and the predicted results are in excellent agreement with the analytical solution. The predicted heat flux by the *D2Q9* lattice is slightly higher than the values predicted from Fourier equation, which can be due to the fictitious high speed diagonal particles that contribute to heat flux (see Eq. (10)). T^* and x^* are defined as $(T - T_c)/(T_h - T_c)$ and x/L , respectively. The material is considered to be silicon; the average physical phonon and bulk properties of silicon at the average temperature of 300 K are presented in [Table 1](#).

4.2. Thermal wave propagation in an infinite medium

To evaluate the performance of the *D2Q7* and *D2Q9* lattice configurations for thermal transport in the ballistic regime, where the Fourier law is not valid, a square domain with periodic boundary conditions on all sides was considered. Material properties were equal to those reported in [Table 1](#). The entire domain, except for a hot region in the middle, was initially set to a temperature of 299.5 K. The hot region in the middle of the domain had a radius of 1/30 of the domain side length, and was initialized to a temperature of 300.5 K. The system was then allowed to evolve in time. The propagation of thermal wave

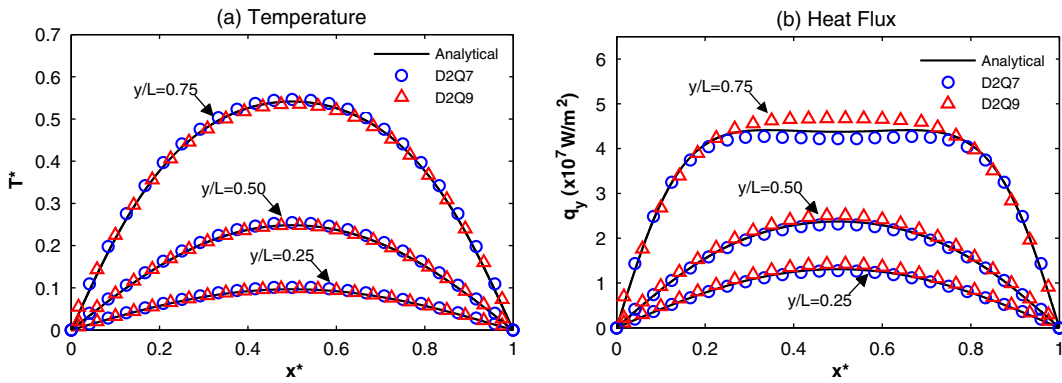


Fig. 4. (a) Temperature and (b) heat flux profile comparison of the analytical Fourier-based solution against the LBM predicted results using the *D2Q7* and *D2Q9* lattices for the diffuse regime.

Table 1

Average physical phonon and bulk properties for silicon at 300 K.

Phonon relaxation time (τ)	6.53×10^{-12} s
Phonon mean free path (λ)	41.79×10^{-9} m
Phonon group velocity (v_g)	6400 m/s
Phonon frequency (ω)	8.18×10^{13} rad/s
Volumetric specific heat (c_v)	1.66×10^6 J/m ³ K
Density (ρ)	2328 kg/m ³
Bulk thermal conductivity (k)	148 W/mk

from the hot region into the cold infinite domain was simulated for five different domain side lengths between 30 nm and 3000 nm (i.e., 30, 100, 300, 800, and 3000 nm); which correspond to initial hot region radii ranging between 1 nm and 100 nm, respectively. The required lattice resolution for a lattice-independent transient prediction of the temperature field is almost as demanding as the required lattice resolution for heat flux predictions.

The simulation results for different hot region radii are presented in Fig. 5 in the form of temperature filled-contours. The corresponding time of all the temperature fields shown in Fig. 5 is equal to $0.2L/v_g$, where L is the domain side length. For domain lengths comparable to or smaller than the phonon mean free path (e.g., Fig. 5(a) and (f)), the traveling time is smaller than the phonon relaxation time; therefore, intrinsic phonon scattering is not significant and phonons travel ballistically to a distance of $0.2L$ at the specified group velocity. In this ballistic regime, the two lattices perform significantly different due to the fictitious high speed phonons on the diagonal directions of the *D2Q9* lattice. The phonons, which are assumed to have isotropic properties in the Gray approximation, propagate anisotropically on the *D2Q9* lattice. In this regime, however, there is little or no communication (diffusion through scattering) between the discretized lattice directions. As a result, we also observed that for both lattices the effect of direction discretization becomes apparent, which is an inherent downfall of the LBM for phonons. Graham [57] also has reported similar patterns for temperature and heat flux profiles when the characteristic size of their computational domain was comparable to the phonon mean free path. They compared their LBM predicted results against those obtained from the discrete ordinate method (DOM) [58,59], and observed that the DOM also yields a very coarse temperature profile in ballistic regime, if the number of propagation directions for phonons are not sufficient. This issue is common in any numerical method when a limited number of discrete propagation directions are selected to represent a continuous scattering process. In the radiative heat transfer literature, this effect was noted by Chai et al. for transparent media [60], when DOM was used to model photon transport, and it has been referred to as ray effect since then [61–63].

If one does not make the isotropic assumption for the mode-dependent phonon properties, the symmetry of the numerical lattices breaks due to different phonon velocities in different directions. In this case, each phonon mode travels on its specific lattice with a mode-dependent lattice skewness due to different degrees of anisotropy for each mode. As a result, the combination of all these lattices covers a larger number of propagation directions in space. This consequently mitigates the ray effect observed in the pure ballistic transport regime. At each time step, all the phonon modes should be mapped into a reference lattice for the collision step, which is a computationally expensive task and requires two-dimensional interpolation in space for each phonon mode.

As presented in Fig. 5, when the domain size increases to values larger than the phonon mean free path, the elapsed time required for traveling a distance of $0.2L$ increases, and becomes larger than the phonon relaxation time. As this occurs, phonons will have a greater likelihood of collision due to intrinsic phonon–phonon scattering, resulting in a transition to a dif-

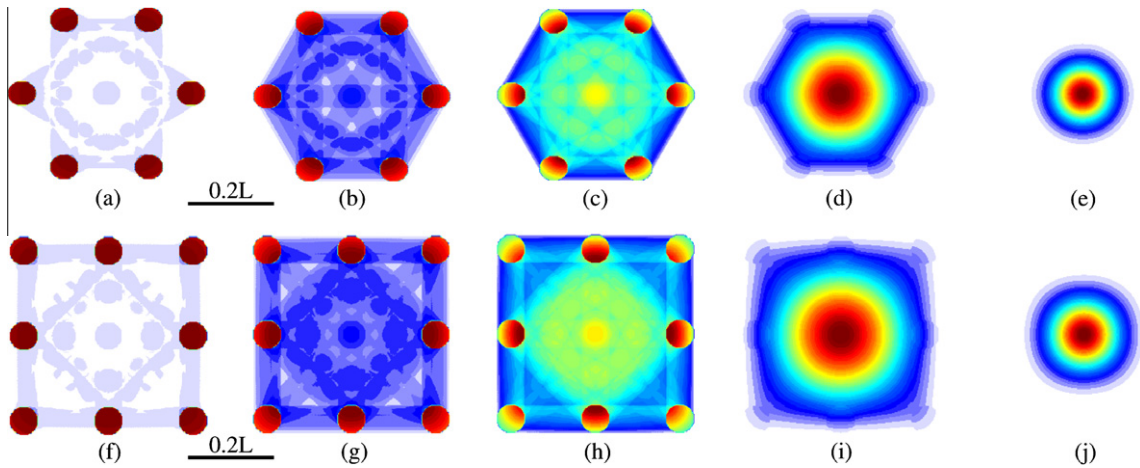


Fig. 5. Dissipation of heat from a high temperature region into a cold infinite domain with periodic boundary conditions, for 5 different domain sizes of (a,f) 30, (b,g) 100, (c,h) 300, (d,i) 800, and (e,j) 3000 nm at $t = 0.2L/v_g$. Simulations are performed using the $D2Q7$ (a to e) and $D2Q9$ (f to j) lattices.

fusive (i.e., bulk-like) transport regime. For a relatively large domain size (i.e., 3000 nm), the two lattices illustrate similar temperature profiles; however, due to the fictitious fast phonons on the diagonal directions of the $D2Q9$ lattice, the constant temperature rings are larger for the $D2Q9$ lattice. The $D2Q9$ lattice predicts a faster propagation of heat through the infinite domain, and therefore the decay of the maximum temperature at the center of the initial high temperature region is faster. The predicted maximum temperature using the $D2Q9$ lattice is about 20% lower than that predicted using the $D2Q7$ lattice for a domain side length of 3000 nm at $t = 0.2L/v_g$.

The circular wave fronts observed in Fig. 5(e) and (j) are indicative of diffuse transport, where intrinsic phonon–phonon scattering is dominant. For both lattices, the effective traveling distance of phonons is considerably shorter than $0.2L$ due to the intrinsic scattering.

The transient behavior of the two lattices is different; however, by increasing the domain size, the difference between the transient predictions of the two lattices become increasingly insignificant. The error introduced by the $D2Q9$ lattice in the transient simulations prohibits its use for thermal transport simulations when sub-continuum effects are present. Therefore, for two-dimensional LBM modeling of phonon transport, we recommend that the $D2Q7$ lattice structures should be used. Because there is no detailed work on the implementation of the phonon LBM on a $D2Q7$ lattice in the literature, we provide a comprehensive numerical recipe for such an implementation in Appendices A, B, and C.

5. Summary

When the characteristic length of a device becomes comparable to the mean free path of energy carriers, e.g., phonons in semiconductor and insulator materials, the study of energy carriers is crucial for accurate thermal transport predictions. The lattice Boltzmann method is shown to be a versatile and powerful tool for modeling phonon transport in such materials.

We showed that the anisotropic structure of the $D2Q9$ lattice leads to erroneous results in the ballistic regime, and the use of the $D2Q7$ lattice is preferred for two-dimensional simulations. However, at the ballistic regime, the effect of lattice directional discretization becomes apparent in two-dimensional simulations, which yields coarse temperature and heat flux fields. This is an inherent downfall of the LBM, which is also observed in other methods that use directional discretization to approximate a continuous scattering process.

It was also shown that the physical group velocity of phonons should be corrected to the average projected values in one- and two-dimensional simulations. The correction factors are $1/2$ and $2/\pi$ for one- and two-dimensional simulations, respectively. Although the Gray LBM implementation was discussed in this work for the sake of clarity, the choice of the lattice structure and use of correction factors are also valid for multi-mode isotropic phonon LBM simulation, which is required for a more accurate prediction of thermal transport.

Numerical methodology of the LBM for phonons (Section 2), implementation of the initial condition (Appendix A), and implementation of various boundary conditions (Appendix B) are discussed in detail.

Acknowledgements

The authors acknowledge the financial support from Advanced Micro Devices, Inc. (AMD), Mathematics of Information Technology and Complex Systems (MITACS), and Natural Sciences and Engineering Research Council of Canada (NSERC).

Appendix A. Initial condition

In a Gray LBM simulation, each lattice site is initialized to the equilibrium distribution function at the corresponding initial temperature that is computed from Eq. (2). Initially, we assume that phonons are evenly distributed in space such that their distribution on each direction (α) is the equilibrium distribution divided by the number of discrete directions, as follows:

$$f_{\alpha}^{initial}(\mathbf{x}, t) = f_{\alpha}^{eq}(\mathbf{x}, t) = \frac{f_{\alpha}^{eq}|_{T(\mathbf{x},t)}}{m-1} = \frac{\left(e^{\frac{h\omega}{k_b T(\mathbf{x},t)}} - 1 \right)^{-1}}{m-1} \quad \alpha = 1, \dots, m-1 \tag{A.1}$$

Appendix B. Boundary conditions

B.1. Periodic boundary condition

The periodic boundary condition implies that any phonon which leaves the computational domain enters the domain from the other side without any change. This type of boundary condition is used when dealing with infinite domains with a repetitive pattern or domains which correspond to closed loops. Considering the $D2Q7$ lattice implementation presented in Fig. 3, if one applies the periodic boundary conditions in the x direction, the nodes on the left boundary with odd j index receive the distribution functions f_1, f_2, f_6 from the nodes on the right boundary. The nodes on the left boundary with even j index only receive f_1 from the right boundary nodes. Similar rules can be developed for the right boundary nodes. The unknown distribution functions on boundary lattice sites are marked in Fig. B.6, and are calculated as follows:

$$\begin{aligned} 1, 2, 6(1, 2p-1) &= f_{1,2,6}(nx, 2p-1) & f_4(nx, 2p-1) &= f_4(1, 2p-1) \\ f_1(1, 2p) &= f_1(nx, 2p) & f_{3,4,5}(nx, 2p) &= f_{3,4,5}(1, 2p) \end{aligned} \tag{B.1}$$

where p is an integer. Similar relations for periodic boundary condition in the y direction can be easily developed by the reader.

B.2. Constant temperature boundary condition

Constant temperature boundary conditions are implemented by setting the distribution function of the boundary nodes equal to the equilibrium distribution function corresponding to the prescribed temperature at that boundary calculated from Eq. (2). These populations are not updated during the streaming step and do not go under collision.

B.3. Constant heat flux boundary condition

On a boundary node with a prescribed heat flux, the phonon distributions which are entering the domain are calculated based on the incoming phonons from inside the domain and the prescribed value of heat flux on that node. These boundary nodes go under collision and their distribution functions are updated at each time step. However, as a general rule, heat flux on any boundary node should be calculated before the collision step. The collision operator conserves the total energy on each node, and therefore conserves the temperature, but does not conserve the heat flux. For the $D1Q3$ lattice, when a prescribed heat flux is implemented on the left boundary, $q_{left}(t)$, the unknown incoming distribution function, $f_1(1, t)$, can be calculated using Eq. (10), as follows:

$$f_1(1, t) = f_2(1, t) + \frac{q_{left}(t)}{q_{factor}} \tag{B.2}$$

For a two-dimensional $D2Q7$ lattice, constant heat flux boundary condition treatment for the top/bottom and left/right boundaries is different due to the different number of directions involved. For the cell orientation and constant i line shown in Fig. 3, constant heat flux condition on the top boundary yields:

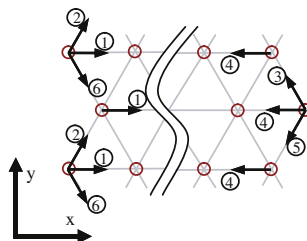


Fig. B.6. Unknown distribution functions for periodic boundary condition in the x direction for $D2Q7$ lattice.

$$q_{y,top}(i, ny, t) = q_{factor}[f_5(i, ny, t) + f_6(i, ny, t) - f_2(i, ny, t) - f_3(i, ny, t)]\cos\frac{\pi}{6} \tag{B.3}$$

where f_5 and f_6 , are the unknown distribution functions on the boundary nodes. The symmetry of the lattice implies that:

$$f_5(i, ny, t) = f_6(i, ny, t) \tag{B.4}$$

Therefore, the two unknown distribution functions are calculated as follows:

$$f_{5,6}(i, ny, t) = \frac{1}{2} \left[\frac{q_{y,top}(i, ny, t)}{q_{factor}} \frac{2}{\sqrt{3}} + f_2(i, ny, t) + f_3(i, ny, t) \right]$$

A similar relation can be developed for the two unknown distribution functions on a constant heat flux boundary on the bottom boundary, i.e., f_2 and f_3 . However, for a constant heat flux condition on the left boundary, the heat flux equation, Eq. (10), reads:

$$q_{x,left}(1, j, t) = q_{factor} \left(f_1(1, j, t) - f_4(1, j, t) + [f_2(1, j, t) + f_6(1, j, t) - f_3(1, j, t) - f_5(1, j, t)]\cos\frac{\pi}{3} \right) \tag{B.5}$$

where f_1, f_2 , and f_6 are the three unknown distribution functions for the boundary nodes with odd j index; while the only unknown distribution function for the boundary nodes with even j index is f_1 . For a boundary node with an odd j index, it can be assumed that the phonons are emitted uniformly in all directions from the boundary node; therefore, one can write:

$$f_1(1, j, t) = f_2(1, j, t) = f_6(1, j, t) \tag{B.6}$$

Combining Eqs. (B.5) and (B.6) yields:

$$f_{1,2,6}(1, j, t) = \frac{1}{2} \left(\frac{q_{x,left}}{q_{factor}} + f_4(1, j, t) + \frac{1}{2} [f_3(1, j, t) + f_5(1, j, t)] \right) \tag{B.7}$$

For the boundary nodes with even j index, the only unknown distribution, f_1 , is calculated by interpolating between the two neighbor nodes, as follows:

$$f_1(1, j, t) = \frac{1}{2} [f_1(1, j - 1, t) + f_1(1, j + 1, t)] \tag{B.8}$$

B.4. Adiabatic boundary condition

It is known that when phonons hit a domain boundary, a portion of them is reflected back, a portion is absorbed, and the rest of them transmit through the boundary. For an ideal adiabatic boundary, every phonon which hits the boundary will be reflected back into the domain and the bins of the absorbed and transmitted phonons will be empty. An ideal reflecting boundary condition can be treated in two different ways, namely: diffuse and specular reflections [37,53]. The unknown outgoing distributions are based on the incoming distributions and are calculated differently in each of these two methods. Fig. B.7 shows the unknown distribution functions for adiabatic boundaries on the top and left boundaries of a two-dimensional domain with D2Q7 lattice implementation.

For the diffuse reflection, it is assumed that incoming populations will be divided equally between the outgoing populations, which are reflected back to the domain. Implementing this type of boundary condition on the left and top boundaries yields:

Top boundary:

$$f_5 = f_6 = \frac{1}{2} [f_2 + f_3] \tag{B.9}$$

Left boundary:

$$f_1 = f_2 = f_6 = \frac{1}{3} [f_3 + f_4 + f_5] \tag{B.10}$$

The diffuse reflection assumption on an adiabatic boundary conserves energy and therefore temperature, but does not necessarily guarantee a zero heat flux.

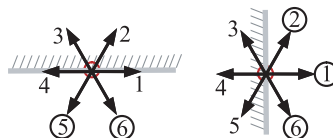


Fig. B.7. Unknown distribution functions for adiabatic boundary condition implementation on the top and left boundaries.

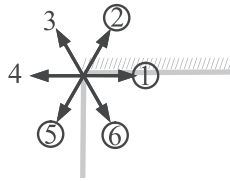


Fig. B.8. A node at the corner of constant temperature (left) and adiabatic (top) boundaries.

In a specular reflection, phonons which hit the boundary will be reflected back into the domain with the same tangential velocity before the collision, but their normal velocity is reversed. A specular adiabatic boundary condition on the left and top boundaries is implemented as follows:

Top boundary:

$$f_5 = f_3, \quad f_6 = f_2 \quad (\text{B.11})$$

Left boundary:

$$f_1 = f_4, \quad f_2 = f_3, \quad f_6 = f_5 \quad (\text{B.12})$$

For both the diffuse and specular treatments on the left boundary, the only unknown distribution on nodes with even j index (f_i) is calculated by interpolation between the top and bottom neighboring nodes, as explained in Eq. (B.8). Specular treatment of an adiabatic boundary condition conserves energy, and enforces zero heat flux at the boundary.

B.5. Corner nodes

Treatment of the nodes at the corners of the domain (or generally at the intersection of any two distinct boundary conditions) should be performed with extra care. To exemplify such a case, a node at the corner of constant temperature (left) and adiabatic (top) boundary conditions is presented in Fig. B.8. Distributions f_3 and f_4 are the incoming distributions from the neighboring nodes. Distributions f_1, f_2, f_5 , and f_6 are the four unknowns. For such a corner node, f_1 and f_2 are determined with respect to the constant temperature boundary condition following the procedure explained in Appendix B.2. The remaining two unknown distribution functions, f_5 and f_6 , are then calculated using the adiabatic boundary condition. These two unknown distributions are set equal to f_3 and f_2 , respectively, if one uses the specular adiabatic boundary treatment to ensure zero heat flux in the y direction on this node.

Appendix C. Streaming

Streaming relations for the $D2Q7$ lattice depends on the choice of the unit hexagonal cell orientation and the form of the constant i and constant j lines. For the cell orientation presented in Fig. 3, the streaming relations for the odd and even j index nodes are different. For the nodes with odd j index, the streaming rules are given as follows:

$$\begin{aligned} f_1(i,j) &= f_1(i-1,j), & f_2(i,j) &= f_2(i-1,j-1) \\ f_3(i,j) &= f_3(i,j-1), & f_4(i,j) &= f_4(i+1,j) \\ f_5(i,j) &= f_5(i,j+1), & f_6(i,j) &= f_6(i-1,j+1) \end{aligned} \quad (\text{C.1})$$

and for nodes with even j index, it is formulated as follows:

$$\begin{aligned} f_1(i,j) &= f_1(i-1,j) & f_2(i,j) &= f_2(i,j-1) \\ f_3(i,j) &= f_3(i+1,j-1) & f_4(i,j) &= f_4(i+1,j) \\ f_5(i,j) &= f_5(i+1,j+1) & f_6(i,j) &= f_6(i,j+1) \end{aligned} \quad (\text{C.2})$$

References

- [1] G. Karniadakis, A. Beskok, N. Aluru, *Microflows and Nanoflows: Fundamentals and Simulation*, Springer, New York, 2005.
- [2] G. Chen, *Nanoscale Energy Transport and Conversion: A Parallel Treatment of Electrons, Molecules, Phonons, and Photons*, Oxford University Press, New York, 2005.
- [3] S. Karajgikar, K. Ghose, B. Sammakia, C.H. Amon, G. Refai-Ahmed, Multi-objective optimization to improve both thermal and device performance of a nonuniformly powered micro-architecture, *Journal of Electronic Packaging* 132 (2010) 021008.
- [4] J.M. Ziman, *Electrons and Phonons*, Oxford University Press, New York, 2001.
- [5] K.E. Goodson, Y.S. Ju, Heat conduction in novel electronic films, *Annual Review of Materials Science* 29 (1999) 261–293.
- [6] D.G. Cahill, W.K. Ford, K.E. Goodson, G.D. Mahan, A. Mujumdar, H.J. Maris, R. Merlin, S.R. Phillpot, Nanoscale thermal transport, *Journal of Applied Physics* 93 (2003) 793–818.
- [7] A.A. Joshi, A. Majumdar, Transient ballistic and diffusive phonon heat transport in thin films, *Journal of Applied Physics* 74 (1) (1993) 31–39.
- [8] G. Chen, Ballistic-diffusive heat-conduction equations, *Physical Review Letters* 86 (11) (2001) 2297–2300.

- [9] G. Chen, Ballistic-diffusive equations for transient heat conduction from nano to macroscales, *Journal of Heat Transfer* 124 (2) (2002) 320–328.
- [10] S.V.J. Narumanchi, J.Y. Murthy, C.H. Amon, Submicron heat transport model in silicon accounting for phonon dispersion and polarization, *Journal of Heat Transfer* 126 (6) (2004) 946–955.
- [11] S.V.J. Narumanchi, J.Y. Murthy, C.H. Amon, Comparison of different phonon transport models for predicting heat conduction in silicon-on-insulator transistors, *Journal of Heat Transfer* 127 (7) (2005) 713–723.
- [12] S. Mazumder, A. Majumdar, Monte Carlo study of phonon transport in solid thin films including dispersion and polarization, *Journal of Heat Transfer* 123 (4) (2001) 749–759.
- [13] M.S. Jeng, R. Yang, D. Song, G. Chen, Modeling the thermal conductivity and phonon transport in nanoparticle composites using Monte Carlo simulation, *Journal of Heat Transfer* 130 (4) (2008) 042410.
- [14] Q. Hao, G. Chen, M.S. Jeng, Frequency-dependent Monte Carlo simulations of phonon transport in two-dimensional porous silicon with aligned pores, *Journal of Applied Physics* 106 (11) (2009) 114321.
- [15] S. Succi, *The Lattice Boltzmann Equation for Fluid Mechanics and Beyond*, Oxford University Press, New York, 2001.
- [16] G.R. McNamara, G. Zanetti, Use of the Boltzmann equation to simulate lattice-gas automata, *Physical Review Letters* 61 (20) (1988) 2332–2335.
- [17] S. Succi, R. Benzi, F. Higuera, The lattice Boltzmann equation: a new tool for computational fluid-dynamics, *Physica D: Nonlinear Phenomena* 47 (1–2) (1991) 219–230.
- [18] Y.H. Qian, D. D’Humières, P. Lallemand, Lattice BGK models for Navier–Stokes equation, *Europhysics Letters* 17 (6) (1992) 479–484.
- [19] D. D’Humières, I. Ginzburg, M. Krafczyk, P. Lallemand, L.-S. Luo, Multiple-relaxation-time lattice Boltzmann models in three dimensions, *Philosophical Transactions of the Royal Society A: Mathematical, Physical and Engineering Sciences* 360 (1792) (2002) 437–451.
- [20] R. Benzi, S. Succi, M. Vergassola, The lattice Boltzmann equation: theory and applications, *Physics Report* 222 (3) (1992) 145–197.
- [21] S. Chen, G.D. Doolen, Lattice Boltzmann method for fluid flows, *Annual Review of Fluid Mechanics* 30 (1998) 329–364.
- [22] R. Guyer, Phonon gas: a lattice Boltzmann description, *Physical Review E* 50 (6) (1994) 4596–4608.
- [23] W. Jiaung, J. Ho, Lattice Boltzmann study on size effect with geometrical bending on phonon heat conduction in a nanoduct, *Journal of Applied Physics* 95 (3) (2004) 958–966.
- [24] W. Jiaung, J. Ho, Lattice-Boltzmann modeling of phonon hydrodynamics, *Physical Review E* 77 (6 Pt 2) (2008) 066710.
- [25] J.-Y. Yang, L.-H. Hung, Lattice Uehling–Uhlenbeck Boltzmann–Bhatnagar–Gross–Krook hydrodynamics of quantum gases, *Physical Review E* 79 (2009) 056708.
- [26] E.A. Uehling, G.E. Uhlenbeck, Transport phenomena in Einstein–Bose and Fermi–Dirac gases. I, *Physical Review* 43 (1933) 552–561.
- [27] E.A. Uehling, Transport phenomena in Einstein–Bose and Fermi–Dirac gases. II, *Physical Review* 46 (1934) 917–929.
- [28] A.J.C. Ladd, B. Moran, W.G. Hoover, Lattice thermal conductivity: a comparison of molecular dynamics and anharmonic lattice dynamics, *Physical Review B* 34 (1986) 5058.
- [29] A.J.H. McGaughey, M. Kaviani, Quantitative validation of the Boltzmann transport equation phonon thermal conductivity model under the single-mode relaxation time approximation, *Physical Review B* 69 (2004) 094303.
- [30] A.A. Maradudin, A.E. Fein, Scattering of neutrons by an anharmonic crystal, *Physical Review* 128 (6) (1962) 2589–2608.
- [31] M.T. Dove, *Introduction to Lattice Dynamics*, Cambridge University Press, Cambridge, 1993.
- [32] J.E. Turney, E.S. Landry, A.J.H. McGaughey, C.H. Amon, Predicting phonon properties and thermal conductivity from anharmonic lattice dynamics calculations and molecular dynamics simulations, *Physical Review B* 79 (2009) 064301.
- [33] S.S. Ghai, W.T. Kim, R.A. Escobar, C.H. Amon, M.S. Jhon, A novel heat transfer model and its application to information storage systems, *Journal of Applied Physics* 97 (2005) 10P703.
- [34] R.A. Escobar, S.S. Ghai, M.S. Jhon, C.H. Amon, Multi-length and time scale thermal transport using the lattice Boltzmann method with application to electronics cooling, *International Journal of Heat and Mass Transfer* 49 (1–2) (2006) 97–107.
- [35] R.A. Escobar, C.H. Amon, Influence of phonon dispersion on transient thermal response of silicon-on-insulator transistors under self-heating conditions, *Journal of Heat Transfer* 129 (7) (2007) 790–797.
- [36] R.A. Escobar, C.H. Amon, Thin film phonon heat conduction by the dispersion lattice Boltzmann method, *Journal of Heat Transfer* 130 (9) (2008) 092402.
- [37] J.V. Goicochea, Hierarchical modeling of heat transfer in electronic devices., Ph.D. Thesis, Carnegie Mellon University, Pittsburgh, PA, 2008.
- [38] J.V. Goicochea, M. Madrid, C.H. Amon, Phonon relaxation rates in silicon thin films determined by molecular dynamics, in: *Proceedings of Intersociety Conference on Thermal and Thermomechanical Phenomena in Electronic Systems (ITherm)*, 2006.
- [39] J.V. Goicochea, M. Madrid, C.H. Amon, Hierarchical modeling of heat transfer in silicon-based electronic devices, *Journal of Heat Transfer* 132 (10) (2010) 102401.
- [40] B. Thouy, J.P. Mazellier, J.C. Barbe, G. Le Carval, Phonon transport in electronic devices: From diffusive to ballistic regime, in: *International Conference on Simulation of Semiconductor Processes and Devices, Hakone*, 2008.
- [41] B. Thouy, J.P. Mazellier, J.C. Barbe, G. Le Carval, Multiscale phonon transport in electronic devices: from diffusive to ballistic regime, in: *International Conference for Mesoscopic Methods in Engineering and Science*, Amsterdam, 2008.
- [42] P. Heino, Multiscale lattice-Boltzmann finite difference model for thermal conduction from nanoscale hot spots, *International Journal for Multiscale Computational Engineering* 6 (2) (2008) 169–178.
- [43] P. Heino, Role of dispersion and optical phonons in a lattice-Boltzmann finite-difference model for nanoscale thermal conduction, *International Journal for Multiscale Computational Engineering* 6 (4) (2008) 349–360.
- [44] P. Heino, Lattice-Boltzmann finite-difference model with optical phonons for nanoscale thermal conduction, *Computers & Mathematics with Applications* 59 (7) (2010) 2351–2359.
- [45] A. Christensen, S. Graham, Multiscale lattice Boltzmann modeling of phonon transport in crystalline semiconductor materials, *Numerical Heat Transfer, Part B: Fundamentals* 57 (2) (2010) 89–109.
- [46] P.L. Bhatnagar, E.P. Gross, M. Krook, A model for collision processes in gases. I. small amplitude processes in charged and neutral one-component systems, *Physical Review* 94 (3) (1954) 511–525.
- [47] F. Reif, *Fundamentals of Statistical and Thermal Physics*, McGraw Hill, New York, 1965.
- [48] D.P. Sellan, J. Turney, A.J.H. McGaughey, C.H. Amon, Cross-plane phonon transport in thin films, *Journal of Applied Physics* 108 (2010) 113524.
- [49] J. Callaway, Model for lattice thermal conductivity at low temperatures, *Physical Review* 113 (1959) 1046–1051.
- [50] M.G. Holland, Analysis of lattice thermal conductivity, *Physical Review* 132 (1963) 2461–2471.
- [51] A.J.H. McGaughey, M. Kaviani, Observation and description of phonon interactions in molecular dynamics simulations, *Physical Review B* 71 (18) (2005) 184305.
- [52] J.E. Turney, A.J.H. McGaughey, C.H. Amon, In-plane phonon transport in thin films, *Journal of Applied Physics* 107 (2) (2010) 024317.
- [53] R. Escobar, Lattice Boltzmann modeling of phonon transport in silicon films, Ph.D. Thesis, Carnegie Mellon University, Pittsburgh, PA, 2005.
- [54] D.P. Sellan, E.S. Landry, J.E. Turney, A.J.H. McGaughey, C.H. Amon, Size effects in molecular dynamics thermal conductivity predictions, *Physical Review B* 81 (21) (2010) 214305.
- [55] J.R. Lukes, D. Li, X.G. Liang, C.L. Tien, Molecular dynamics study of solid thin-film thermal conductivity, *Journal of Heat Transfer* 122 (2000) 536–543.
- [56] E. Kreyszig, *Advanced Engineering Mathematics*, John Wiley and Sons, New York, 2006.
- [57] S. Graham, Private communications.
- [58] W.A. Fiveland, Discrete ordinate methods for radiative heat transfer in isotropically and anisotropically scattering media, *Journal of Heat Transfer* 109 (3) (1987) 809–812.

- [59] D. Baillis, J. Randrianalisoa, Prediction of thermal conductivity of nanostructures: Influence of phonon dispersion approximation, *International Journal of Heat and Mass Transfer* 52 (11–12) (2009) 2516–2527.
- [60] J.C. Chai, H.S. Lee, S.V. Patankar, Ray effect and false scattering in the discrete ordinates method, *Numerical Heat Transfer, Part B: Fundamentals* 24 (4) (1993) 373–389.
- [61] P.J. Coelho, The role of ray effects and false scattering on the accuracy of the standard and modified discrete ordinates methods, *Journal of Quantitative Spectroscopy and Radiative Transfer* 73 (2–5) (2002) 231–238.
- [62] H.S. Li, G. Flamant, J.D. Lu, Mitigation of ray effects in the discrete ordinates method, *Numerical Heat Transfer, Part B: Fundamentals* 43 (5) (2003) 445–466.
- [63] Z.F. Huang, H.C. Zhou, P.F. Hsu, Improved discrete ordinates method for ray effects mitigation, in: *ASME International Mechanical Engineering Congress and Exposition, IMECE2009*, Lake Buena Vista, FL, 2009.